DEGREE PROJECT, IN MECHANICS , SECOND LEVEL
STOCKHOLM, *SWEDEN 2014*

Modelling and Manufacturing of a Composite Bi-Stable Boom for Small Satellites

FLORIAN HERLEM

KTH ROYAL INSTITUTE OF TECHNOLOGY

ENGINEERING SCIENCES

2014-02-10

ROYAL INSTITUTE
OF TECHNOLOGY

Modelling and Manufacturing of a Composite Bi-Stable Boom for Small Satellites

Florian HERLEM

February 2014

Royal Institute of Technology, Stockholm, Sweden

Main Supervisor
Dr. Gunnar TIBERT

Deputy Supervisor
Mr Pau MALLOL PARERA

Contents

Abstract 1

1 Introduction 3
1.1 KTH's CubeSat projects . . . 3
1.1.1 Overview . . . 3
1.1.2 The SWIM project . . . 4
1.1.3 The SEAM project . . . 4
1.2 Deployable structure background . . . 5
1.3 Aims and objectives . . . 7

2 Material Model 9
2.1 Bi-stability of the tape spring . . . 9
2.2 ABD matrix and laminate layup configurations . . . 10
2.3 Woven model . . . 12

3 Preliminary Tests 17
3.1 Difference between theoretical and real coiling radius . . . 17
3.2 Influence of time . . . 18
3.2.1 Influence of repeted coiling . . . 18
3.2.2 Influence of relaxation . . . 18
3.3 Blooming radius . . . 19
3.4 Preliminary testing conclusion . . . 20

4 Manufacturing of New Tape Springs 21
4.1 Materials data . . . 21
4.1.1 Glass fiber . . . 21
4.1.2 Resin . . . 22
4.1.3 [+45F/−45F/0F/+45F/−45F] layup . . . 22
4.1.4 [+45F/−45F/+45F/−45F/0F/+45F/−45F/+45F/−45F] layup 23
4.2 Vacuum molding procedure . . . 23
4.2.1 Cutting . . . 23
4.2.2 Assembling the layers . . . 24
4.2.3 Adding the resin . . . 25
4.2.4 Molding . . . 25
4.2.5 Post curing . . . 26
4.3 Observations and improvements . . . 27

5 Next Generation of Glass Fiber tape springs **29**
5.1 Why making a new tape spring? 29
5.1.1 Deployment issue 29
5.1.2 Relation between coiling radius and fiber orientation 30
5.2 What will it change? 31
5.2.1 Deployment force and time 31
5.2.2 Equivalent isotropic Young's modulus 33

6 Conclusion **35**

Acknowledgments **37**

Bibliography **39**

Abstract

Thin cylindrical shell structures may provide an interesting breakthrough for deployable structures for small satellites. Its bi-stable behaviour allows two different stable configurations: coiled and deployed. Several projects worldwide are using tape springs for satellites and for the SEAM project, at KTH, 1 meter long tape springs will be used for booms.

This thesis investigates the energy stored inside the tape spring according to its layup configuration and the different fiber orientations. With a thickness around 0.3 mm and a length of one meter, the booms will deploy sensors with a quite low deployment speed in order to minimize the shick load during the deployment phase. A Matlab code is written to compare the stored strain energy. Another aim is to find an adequate layout all along the tape spring, it means change the fiber orientation to decrease the energy released, but also generating main manufacturing issue.

Keywords: bi-stable, deployable boom, composite materials.

1 Introduction

1.1 KTH's CubeSat projects

1.1.1 Overview

A CubeSat is a nano-satellite for space research, usually around one liter volume and a maximum mass of 1.33 kg. It was firstly developed in 1999 by California Polytechnic State University and Stanford University. They developed the CubeSat specifications to help universities worldwide to perform space science and exploration.

CubeSats are particularly interesting for academia, small companies or even governments. Typically made from commercial off-the-shelf components, CubeSats enable "space for all". Up until February 2014, more than one hundred CubeSats have been launched [1]. They are commonly launched into Low Earth Orbit by small to medium launchers, e.g. Russian Rokot, Dnepr-1 and US Falcon 9. Unfortunately there have been 28 fails, so around a quarter of failures since 2003.

The standard design of a CubeSat is one unit, 1U, which represents $0.1 \times 0.1 \times 0.1$ m^3 and bigger structures exist up to 6U.

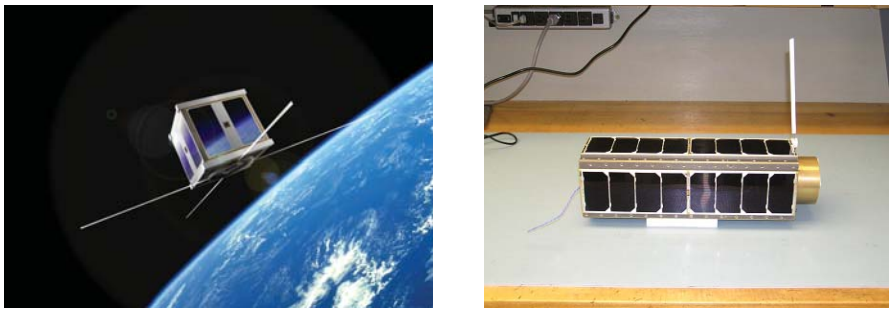

Figure 1.1: AAU CubeSat and GeneSat-1,[2, 3].

CubeSats represent a new way of getting a payload into orbit. Most CubeSats carry only one or two scientific instruments as their primary mission payload. These small satellites have different aims from space weather observation to detection of exoplanet. Indeed their advantages remain low cost, launch opportunity and rapid development time.

1.1.2 The SWIM project

The SWIM project is a CubeSat project led by the University of Puerto Rico (IUPR), University of Florida (UF), Virginia Polytechnic Institute and State University (VT) and the Royal Institute of Technology, Stockholm (KTH), with the aim of bringing a CubeSat from prototype to flight stage.

The actors of this project each specialize in a separate domain. IUPR develops the embedded electronic hardware and software while UF, VT and KTH, together with the United States Air Force Research Laboratory (AFRL) develop the attitude control and deployable structural booms for the sensor payload developed at KTH.

The mission is to deploy the 3U satellite onto a 600 km circular polar orbit. The payload would have a mass of 3.64 kg (including 0.22 m^2 solar array), the instrument is a magnetometer which should deploy correctly (less than 5° error). Interferences produced by the satellite should be negligible compared to the Earth electro-magnetic field, that is why the sensor has to be relatively far away from the electronics and metallic parts of the satellite. The minimum distance is estimated to be one meter for reliable measurements. Therefore a non-metallic deployable structure e.g. a boom one meter long is needed to carry the sensor, and this structure should be stiff and dimensionally stable to avoid angle errors.

Figure 1.2: Small Magnetometer in Low mass Experiment (with the courtessy of SMILE project), [4].

1.1.3 The SEAM project

The SEAM project is another 3U CubeSat project led by the Royal Institute of Technology, Stockholm (KTH), in cooperation with a consortium of companies like ÅAC Microtec, ECM-Office, Laboratory for Electromagnetic Innovations (LEMI), BL-Electronics, GomSpace, the Swedish Space Corporation (SSC) and Kayser Italia. The goal is similar to the SWIM project but using this time two sensors, one on each side of the satellite.

The consortium will develop and demonstrate in flight for the first time a concept of an electromagnetically clean nano-satellite with precision attitude determination,

flexible autonomous data acquisition system, high-bandwidth telemetry and an integrated solution for ground control and data handling [5].

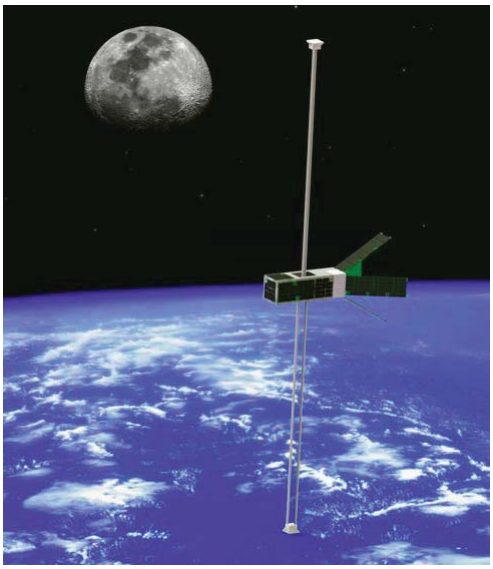

Figure 1.3: SEAM satellite (with the courtesy of SEAM project), [5].

1.2 Deployable structure background

Inside launch vehicle, the satellite or payload has to be compact and light, but when it reaches space it should be as large as needed for the mission. Solar panels and antennas are examples of structures deployed in space.

According to Mikulas [6], there are three main criteria leading the development of such structures, which are mass, stiffness and volume. In CubeSat projects, it seems obvious to consider volume first because of the 1 dm^3 box the structure must fit in. The existing technologies [7] include: foldable beam, telescopic beam, thin walled tubular booms like Storable Tubular Extensible Member (STEM), which is similar to the deployable structure studied in this project.

STEM tubes are thin-walled shell material that can be elastically collapsed and reeled around a cylindrical hub or drum. The tubes can have very different cross-sections, depending on the stiffness required. They are also known as tapes for their resemblance with them.

When the tape is coiled the material stores strain energy thanks to bending and stretching. During the deployment phase, the tape spring goes back to a practically unstressed configuration, creating a high stiffness tubular shape, typically overlapping to increase the shear and torsional stiffness. The strain energy released by the tape spring drives the deployment. If the deployment is not well controlled, STEM

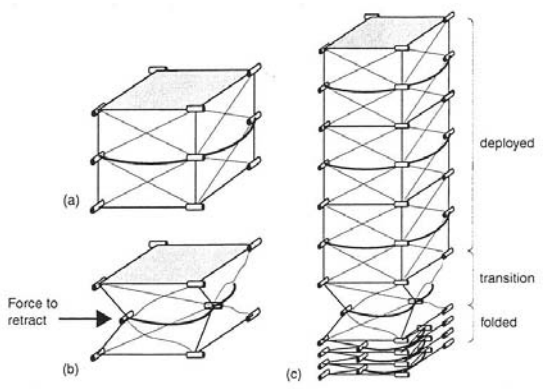

Figure 1.4: Classic tensegrity structure, [7].

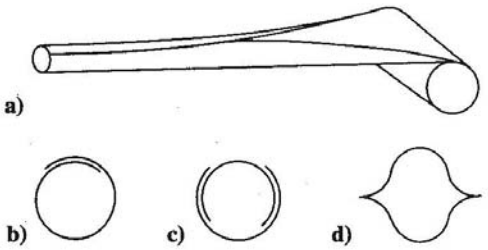

Figure 1.5: STEM types, [7].

booms will deploy in a highly dynamic, uncontrolled and difficult to predict manner. The velocity of the deploying end of the boom accelerates and suddenly stops when the deployment is completed. This impact increases the risk for boom failure or even spacecraft damage. Once the tape spring is entirely deployed, a locking system maintains the deployed state and the whole structure becomes rigid. Materials commonly used for the shells are Beryllium Copper, Stainless Steel, Glass Fiber Reinforced Plastics (GFRP) and Carbon Fiber Reinforced Plastics (CFRP).

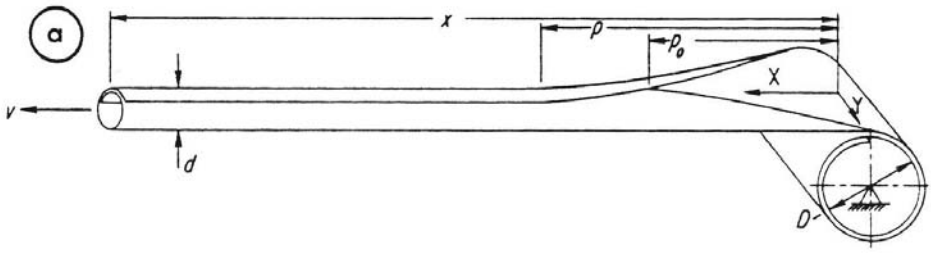

Figure 1.6: STEM deployment, [7].

1.3 Aims and objectives

In this master thesis project, a complete material evaluation is the objective. The first task is to evaluate a GFRP tape spring. It means develop an adequate code which allows us to compare theory and reality of the tape springs, through numerical calculations. Using the laminate theory [8], the ABD matrix and stored energy are computed. Another aim is to adapt the laminate layup, one way is to change the fiber orientation [9] all along the tape spring to propose another solution for deployable structures and which will be used for further analysis.

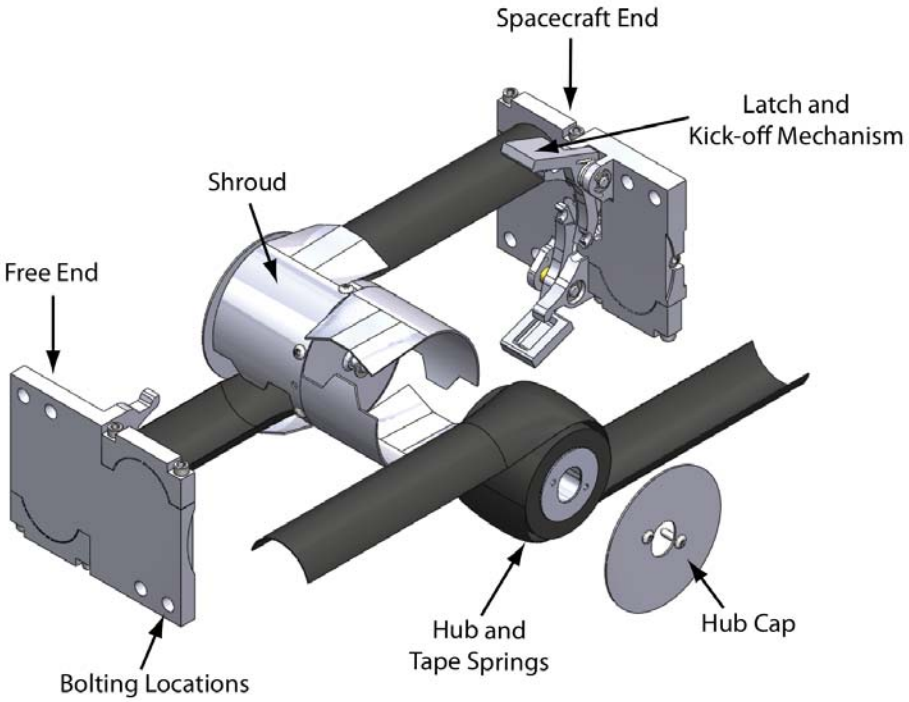

Figure 1.7: Exploded hub view of the SIMPLE boom in initial stages of deployment, [10].

In this paper, all the concepts behind the development of the material model are explained. Then, this model is applied to the boom and to the simulations which give some preliminary results which will be compared with several manufactured samples. Finally, a proposal for the desired boom is made, in terms of energy, forces, geometry, manufacturing, properties, which leads to a discussion about future improvements.

2 Material Model

2.1 Bi-stability of the tape spring

Bi-stability in structural mechanics is a quite young field which consists in a capability of changing the Gaussian curvatures from one position to an other. The tape springs are bi-stable when they actually have two stable configurations which correspond to two different local minima, from the stored strain energy point of view.

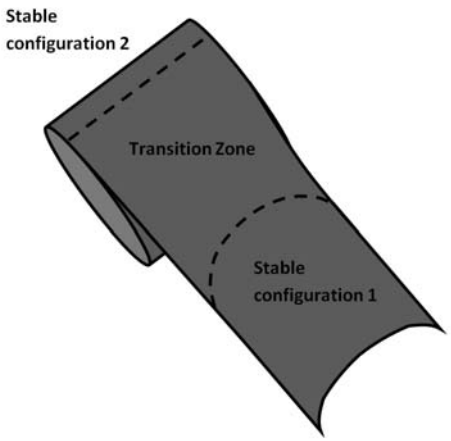

Figure 2.1: The three zones of the tape spring during deployment (courtesy of Yoann Prigent), [11].

The more stable state is when the boom is not coiled as there is no energy stored. When it is coiled, the local energy minimum contains non-zero energy. The transition between the less stable state to the more stable state is feasible by adding a sufficient amount of energy called activation energy. So the stored strain energy will be released into kinetic energy during the snap-through, which is interesting to control.

The models used have been developed by Iqbal & Pellegrino [12] and Guest & Pellegrino [13]. They formulated the theory of composite tape springs.

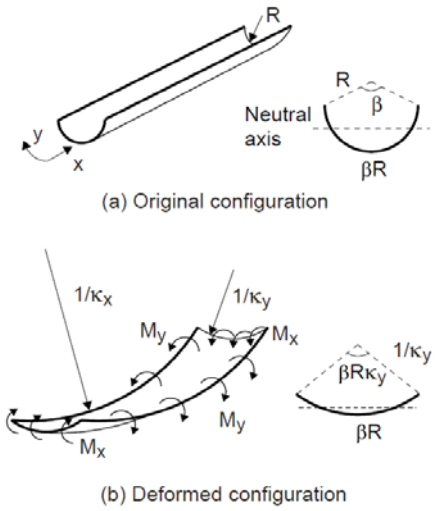

Figure 2.2: Bending and geometry definition (courtesy of Iqbal & Pellegrino), [12].

2.2 ABD matrix and laminate layup configurations

To make the connection between stress and strain, the laminate theory uses the ABD matrix. More precisely, it relates the mid-surface strains and curvatures to the corresponding stress resultants in the shell. One should notice that the x-axis and y-axis to coincide with the longitudinal and transverse directions of the shell, respectively.

$$\begin{bmatrix} \boldsymbol{N} \\ \boldsymbol{M} \end{bmatrix} = \begin{bmatrix} \boldsymbol{A} & \boldsymbol{B} \\ \boldsymbol{B} & \boldsymbol{D} \end{bmatrix} \begin{bmatrix} \boldsymbol{\epsilon^0} \\ \boldsymbol{\kappa} \end{bmatrix} \tag{2.1}$$

To test the code, the materials used by Guest and Pellegrino [13] with a $[+45/-45/0/+45/-45]$ layup were tested. It is composed of five layers of GF and polypropylene (PP) for a total thickness of 1.05 mm. It leads to this ABD matrix (in GN and mm) below, where only significant terms remain.

$$\begin{bmatrix} \boldsymbol{A} & \boldsymbol{B} \\ \boldsymbol{B} & \boldsymbol{D} \end{bmatrix} = \begin{bmatrix} 13.3 & 6.06 & 0 & 0 & 0 & -0.551 \\ 6.06 & 8.06 & 0 & 0 & 0 & -0.551 \\ 0 & 0 & 6.23 & -0.551 & -0.551 & 0 \\ & & & & & \\ 0 & 0 & -0.551 & 0.868 & 0.666 & 0 \\ 0 & 0 & -0.551 & 0.666 & 0.849 & 0 \\ -0.551 & -0.551 & 0 & 0 & 0 & 0.682 \end{bmatrix}$$

The ABD matrix is actually antisymmetric. So there is neither coupling between normal and shear (A_{16} and A_{26}), nor between bending and twisting (D_{16} and D_{26}) but the coupling between bending and stretching (B_{16} and B_{26}) is not zero even if

its behaviour has only a weak effect on the bi-stability of the shell. The laminate plate equations define the force and moment in the plate:

$$\boldsymbol{N} = \int_{-h/2}^{h/2} \boldsymbol{\sigma}\, dz \qquad\qquad \boldsymbol{M} = \int_{-h/2}^{h/2} \boldsymbol{\sigma}\, z dz \tag{2.2}$$

The strain energy is assumed to be the energy from bending and from stretching in the mid-surface. Because of the existing coupling between bending and stretching, in an anisotropic plate, one must integrate the strain energy density through the thickness.

$$U = \frac{1}{2}\int_{-h/2}^{h/2} \boldsymbol{\sigma}^T(\boldsymbol{\epsilon^0} + z\boldsymbol{\kappa})\, dz = \frac{1}{2}(\boldsymbol{\epsilon^{0T}} A \boldsymbol{\epsilon^0} + 2\boldsymbol{\kappa}^T B \boldsymbol{\epsilon^0} + \boldsymbol{\kappa}^T D \boldsymbol{\kappa}) \tag{2.3}$$

This leads to the sum of strain energy due to stretching, coupling between bending and stretching and bending. The coupling term will be neglected, according to Iqbal and Pellegrino [12]. So there are two different sources of strain energy, one from the stretching U_s and one from the bending U_b of the shell. When it comes to strain energy per unit length one should integrate equation (2.3) over the cross section arc-length of βR:

$$\left(\frac{dU}{dL}\right)_s = \frac{A_{11}}{2}\left(\frac{\beta R}{2}\frac{\kappa_x^2}{\kappa_y^2} + \frac{\sin(\beta R \kappa_y)}{2}\frac{\kappa_x^2}{\kappa_y^3} - \frac{4\sin^2(\beta R \kappa_y/2)}{\beta R}\right) \tag{2.4}$$

$$\left(\frac{dU}{dL}\right)_b = \frac{\beta R}{2}\left(D_{11} + 2D_{12}\kappa_x\left(\kappa_y - \frac{1}{R}\right) + D_{22}\left(\kappa_y - \frac{1}{R}\right)^2\right) \tag{2.5}$$

Taking the sum of the stretching and bending energy gives the total strain energy per unit length dU/dL and plotting the energy as function of κ_x and κ_y gives the plots in Fig. 2.3. In Fig. 2.4, there is another type of plot which is also used to look for energy wells (meaning stable area) and it will be developed soon.

When using fabrics instead of unidirectional layer, add an "F" in the laminate code makes the fabric layers notable. The strain energy per unit length plot (Fig. 2.5) is interesting as it gives important information about the tape spring. There are actually two stable points on the graph located : $(\kappa_x, \kappa_y) = (0, R)$ which corresponds to the deployed configuration, where the and $(\kappa_x, \kappa_y) = (R_{\text{coiling}}, \approx 0)$ corresponding to the coiled configuration, in this case $R_{\text{coiling}} = 15.5\,\text{mm}$. On the path from the coiled stable point to the deployed one, it exists a saddle point which has to be "climbed" in order to get from one configuration to the other one, the energy difference between this saddle point and the coiled stable point describes the degree of stability and the impulse energy needed to deploy the structure. The minimum strain path, from coiled to deployed configuration, follows approximatly the gradient of the dU/dL (the dotted lines in Fig. 2.4).

The other method consists in plotting the strain energy through a polar plot. Guest & Pellegrino [13] have developed a simplified model taking only into account the bending strain energy $U = \frac{1}{2}\boldsymbol{\kappa}^T D\boldsymbol{\kappa}$, from equation (2.3). Their work on Mohr's circle, has shown that the curvatures are $\boldsymbol{\kappa} = [\kappa_x, \kappa_y, \kappa_{xy}] = [0, 1/R, 0]$ at the deployed configuration and $\boldsymbol{\kappa} = [\frac{C}{2}(1-\cos 2\theta), \frac{C}{2}(1+\cos 2\theta), \frac{C}{2}\sin 2\theta]$ at the coiled configuration. The bending strain energy can be plotted according to the parameters C and θ. The equilibrium points are found where there are no slope of energy for changes in C and θ.

The polar plots can give other specific properties for symmetric or non-symmetric layup for other fields of application. This method is a close approximation of the total strain energy stored inside the boom. Moreover, since this paper deals with antisymmetric layout, there is no direct need for polar plots in which the corresponding deployed stable point is $[C, 2\theta] = [1, 0]$ and the coiled stable point is located at $[C, 2\theta] = [D_{12}/D_{11}, \pi/2]$.

One advantage of this model is that it gives quickly a very close approximation of the coiling radius.

$$R_{\text{coiling}} = R\frac{D_{11}}{D_{12}} \tag{2.6}$$

2.3 Woven model

To model the woven GF, it was chosen not to use the Naik model [14, 11]. A simpler modelling without gap ratio, consisted in turning one woven layer of the lamina into 16 antisymmetric sub-plies. The interest lies in the fact to trick the computation, as a smaller z difference will almost cancel the coupling matrix. If one divides a woven layer into only 2 antisymmetric sub-plies, a shear-bending or normal-twisting might appear (B_{16} and B_{26}). By dividing the woven layer into 2^4 sub-plies, the B_{16} and B_{26} terms are divided by 4. This method also keeps the bending-twisting, D_{16} term, extremely low (10^{17} times lower than D_{11}). Contrary to a symmetric layup which on the one hand cancels the whole $\boldsymbol{B}$ matrix, but on the other hand keeps the coupling between bending and twisting. This will jeopardise a correct deployment and storage.

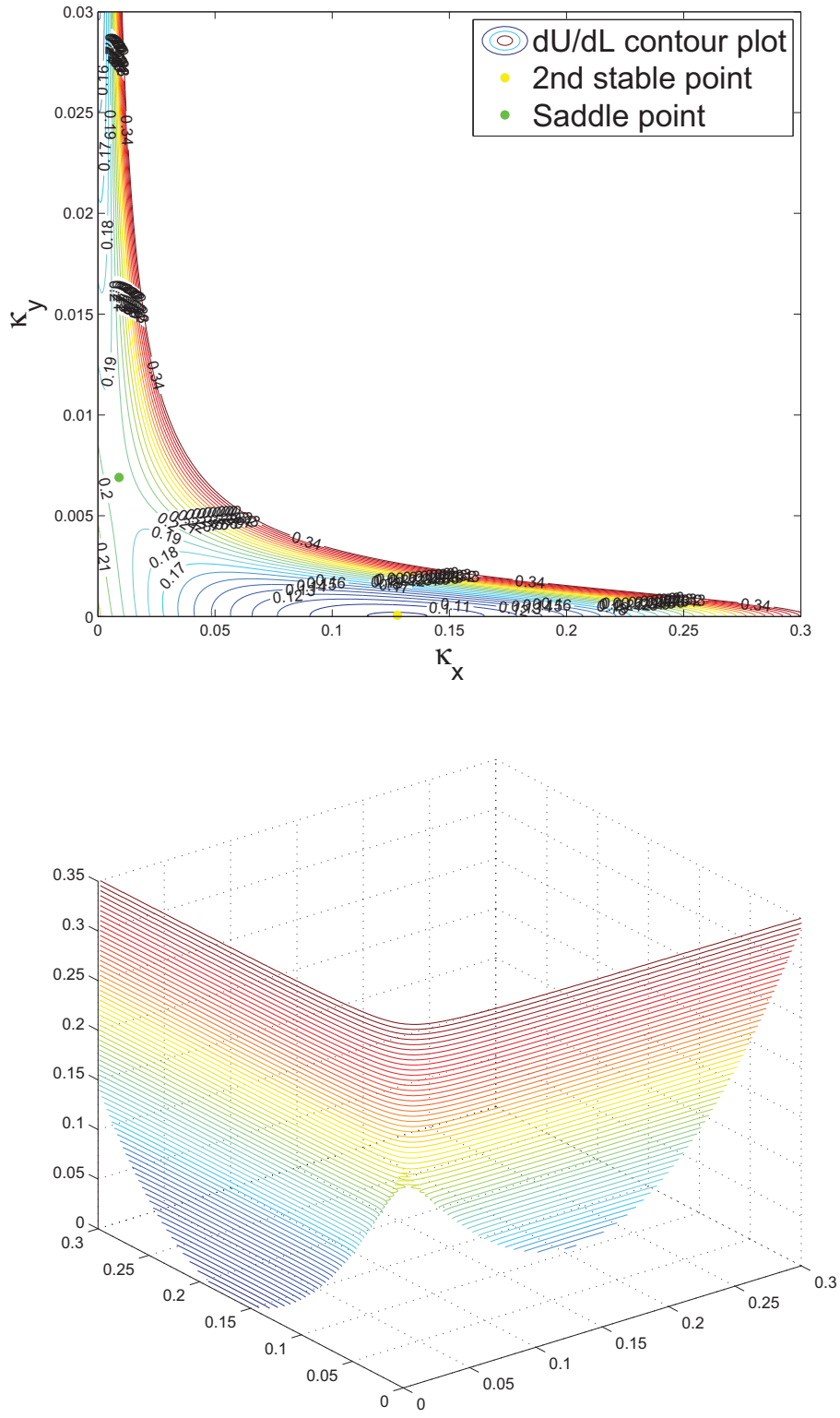

Figure 2.3: Strain energy per unit length plot and strain energy polarplot for [+45/−45/0/+45/−45] layout, $R = 6$ mm.

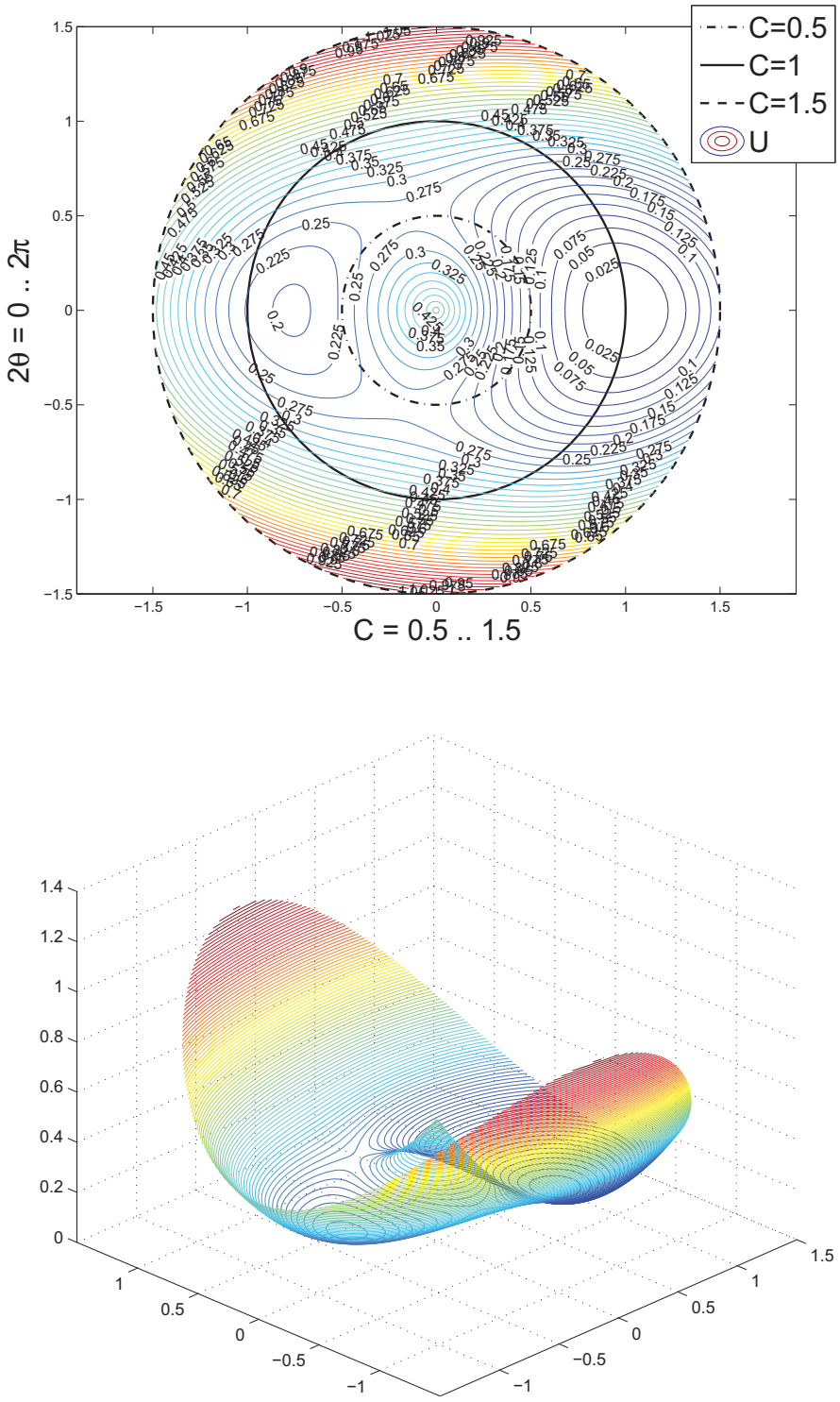

Figure 2.4: Strain energy per unit length plot and strain energy polarplot for $[+45/-45/0/+45/-45]$ layout, $R = 6$ mm.

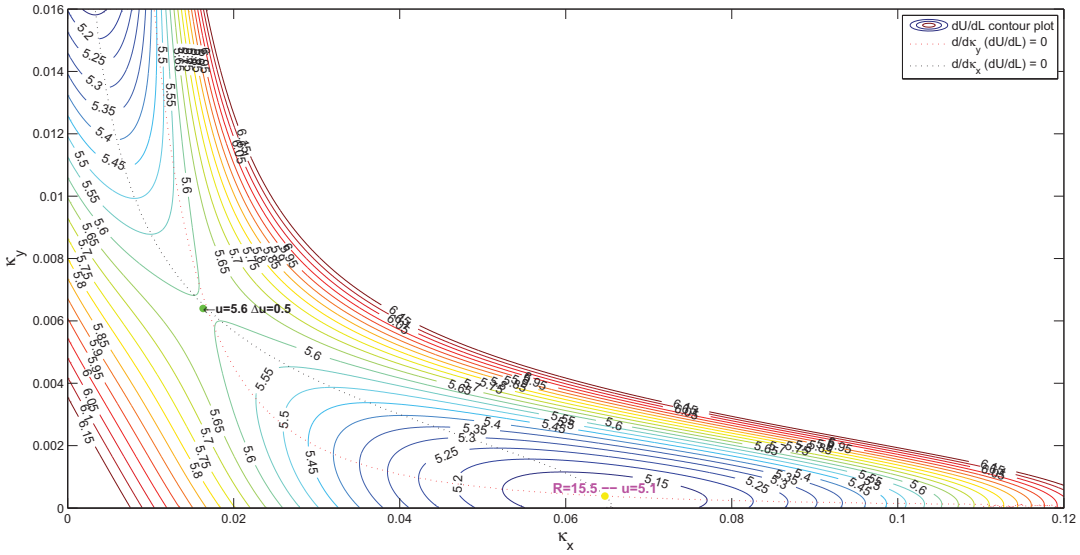

Figure 2.5: Strain energy plot for [±45F/0/±45F] layout, $R = 6.35$ mm.

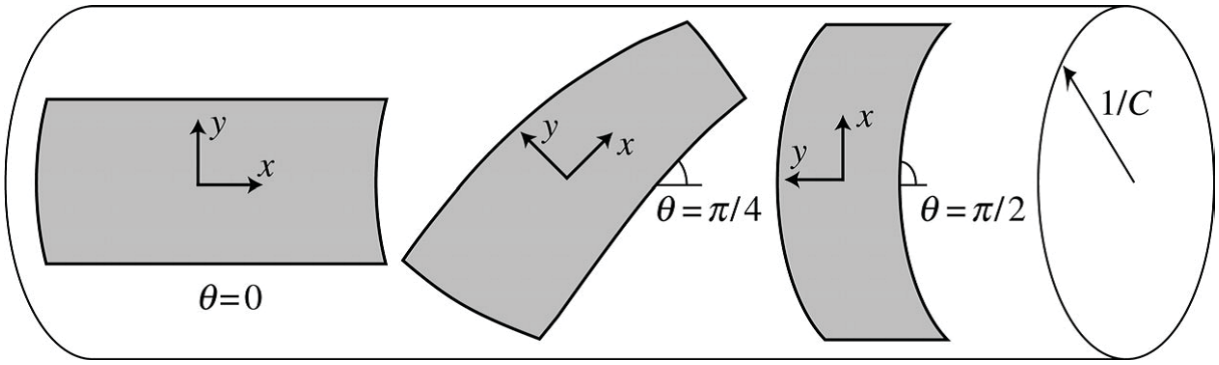

Figure 2.6: Coordinate system where shells are on an underlying cylinder of radius 1/C, [13].

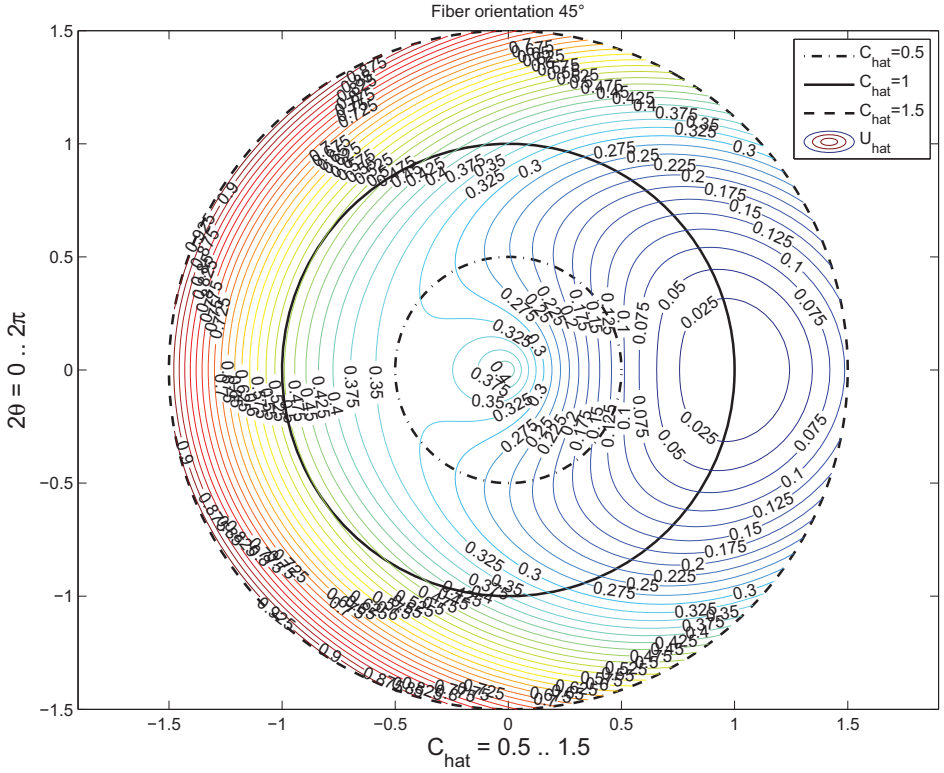

Figure 2.7: Strain energy polarplot for [±45F/0/±45F] layout, $R = 6.35$ mm.

Figure 2.8: Woven model.

3 Preliminary Tests

It was necessary to test the code to know how close it was to reality, so three preliminary tests were conducted to study on the one hand the coiling radius and the impact of time on the tape springs and on the other hand studying the blooming (or snapping) radius to find an operative margin for the diameter of the tape spring when coiled and its properties.

3.1 Difference between theoretical and real coiling radius

It appeared that the computed and the measured coiling radii were not the same. In fact, repeated measurements have shown that the average measured coiling radius was 12.1 mm, instead of 15.5 mm according to the Figure 2.5, or instead of 15.3 mm according to the equation (2.7). The percentage error is 19%, which is quite large, but it corresponds to a difference of 12% of the mechanical properties. Moreover, a range of coiling stability appeared, indeed the radius was measured stable from 11.6 to 12.7 mm, the blue area in Fig. 3.5.

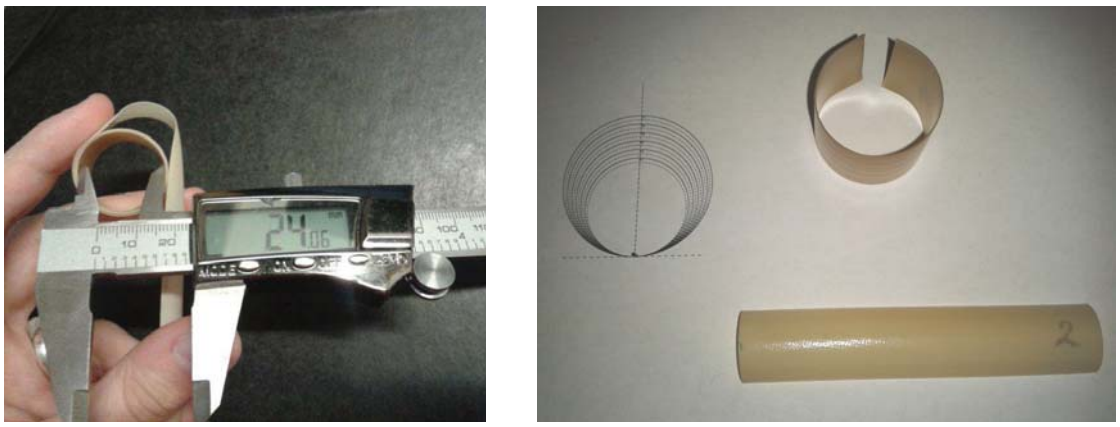

Figure 3.1: Coiling radius measurement by electronic caliper and patterns.

3.2 Influence of time

3.2.1 Influence of repeted coiling

The influence of the repeated coiling manipulations done over the boom was investigated. Thin-walled shell and especially the vinylester matrix which is a polymer is very sensitive to creep [15]. Repeated coiling and deployment starts the creeping process of the matrix which decrease the coiling radius, from 12.4 mm to 11.7 mm, so around 5.6% less which is relatively small.

Table 3.1: Table of the influence of ageing over the boom.

Boom age	Coiling radius (mm)
New (<10 deployments)	12.4
Recent (~50 deployments)	12.0
Old (~250 deployments)	11.7

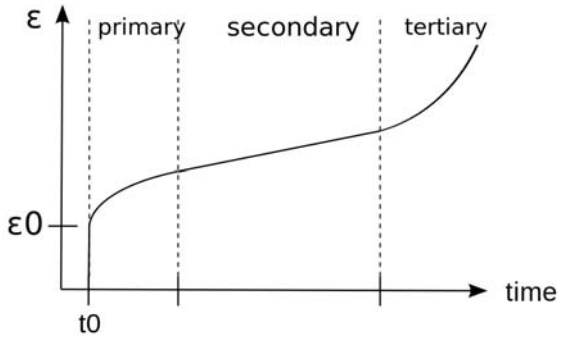

Figure 3.2: Strain as a function of time due to constant stress over an extended period for a viscoelastic material, [16].

3.2.2 Influence of relaxation

Another influence of time is the stress relaxation of the tape spring in the coiled configuration. After several hours, even if the fibers bear most of the load, one may consider the possibility of viscoelasticity. It changes the bi-stability properties since the matrix shall adapt to the new geometry. [17, 15]

Moreover, if the matrix material is used below its glass transition temperature, it will behave in an elastic mode. But, if the laminate copes with elevated temperatures and the fibers are not oriented in the stressed directions, important relaxation effects may be observed. [17]

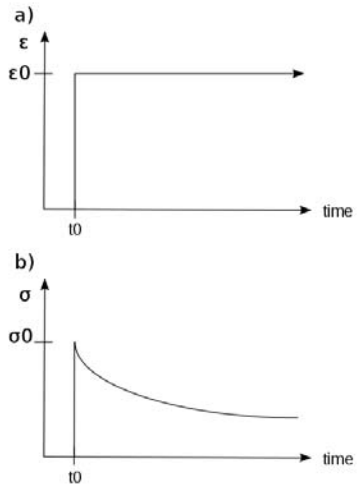

Figure 3.3: Stress relaxation due to constant strain for viscoelastic material, [18].

3.3 Blooming radius

Blooming appears when the coiling radius is too large and the boom wants to deploy. The average blooming radius has been measured to 19.6 mm, or 63% more than the natural coiling radius. It was decided to have more adequate measurement, without the interactions of the other coils, by looking at only one coil limit from blooming, it has been called the "snapping limit" because of the snap-through instability.

As one can see in Fig. 3.4, the aim was to get a radius close to the snapping limit, meaning that a very little perturbation on the coiled tape spring shall make it snap from coiled configuration to initial straight one. The outer part of the clear tape is smooth enough to assume that no friction affects the results.

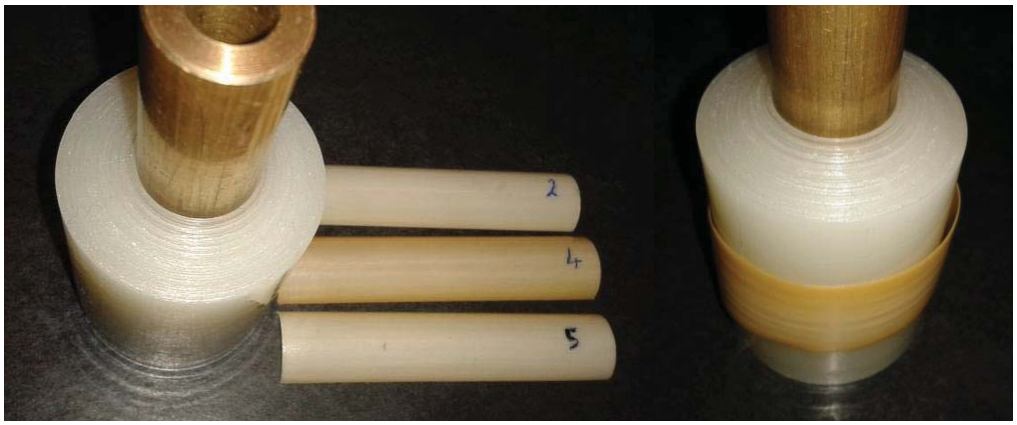

Figure 3.4: Observed snapping limit.

The final diameter of the clear tape was measured with a numerical caliper and the

value was 40.0 mm. One can see, Figure 3.4, that the coil looks a little awkward and a small perturbation makes it snaps immediately. These two observations are quite similar and leads to an increase of 66% from the natural coiling radius of 12.1 mm to the snapping radius of 20.0 mm, for this material and layout.

3.4 Preliminary testing conclusion

After all these tests, a margin is clearly established from natural coiling radius to blooming radius, Fig. 3.5. The boom is naturally coiled in the blue area and when increasing the coiling radius, it does not snap until the red line, the purple line indicates the stable point computed with the Matlab code.

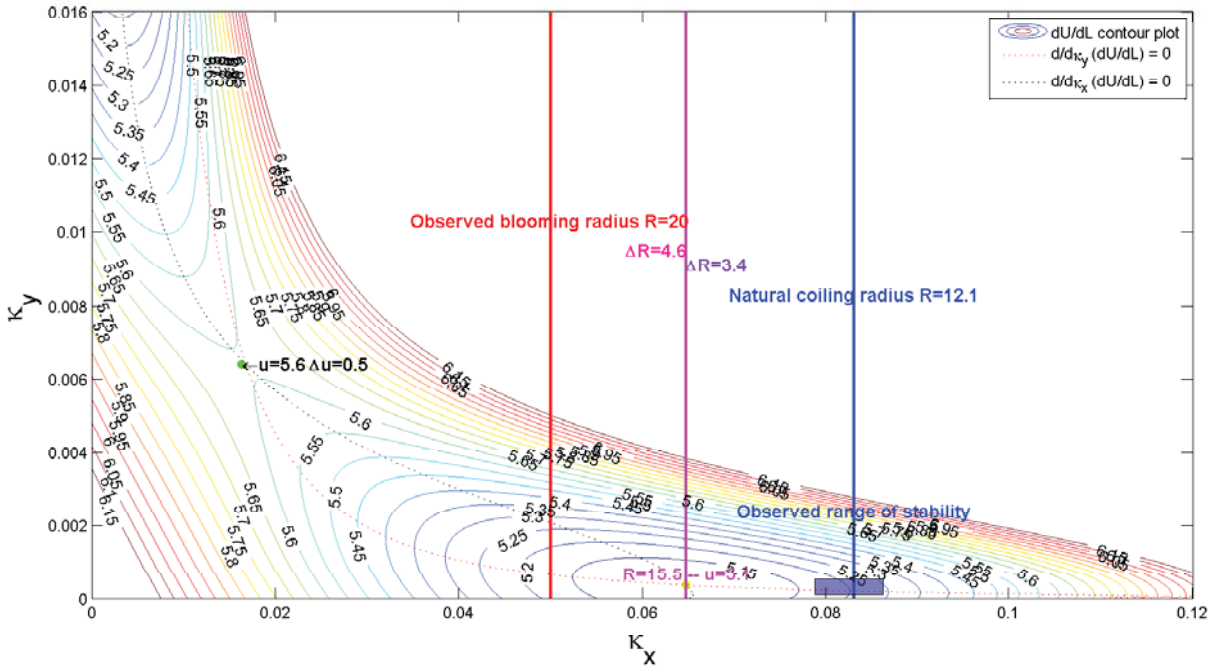

Figure 3.5: Snapping limit observed on energy plot for [±45F/0/±45F] layout, R = 6.35 mm.

The observations suggest that the tape spring is stable between the blue and the red lines. In terms of energy, this total stability range of 8 mm represents a few difference of energy, $\left(\frac{dU}{dL}\right)_2 - \left(\frac{dU}{dL}\right)_1 = 0.15\,\mathrm{N}$, it means that the energy well is large and very flat. Furthermore, the energy well dimensions depends on the materials.

4 Manufacturing of New Tape Springs

A total of four 200 mm samples and one 1-meter tape spring were manufactured in four sessions. The entire process will be developed from cutting the fabrics to the post-curing in the oven.

Since the volume inside the CubeSat is limited, only 25 mm are given for each tape spring width. This width corresponds to the arc-length of the transversal section which means a radius of 8 mm. This is why a copper beam of 1.2 meter and a diameter of 16 mm was used as a mold for manufacturing.

4.1 Materials data

4.1.1 Glass fiber

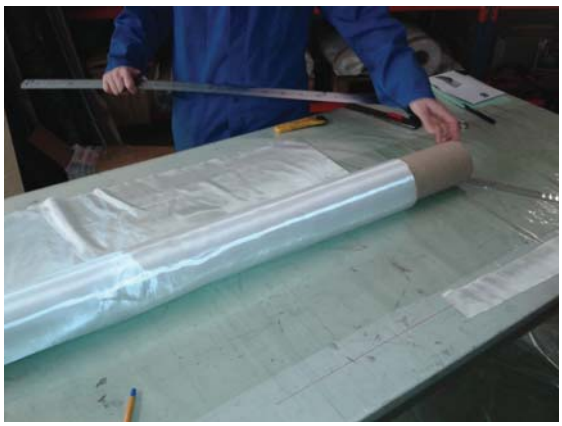

Figure 4.1: Roll of glass fiber fabric.

For the manufacturing study it was decided to take dry glass fiber instead of prepreg because of the rapidity to get fabrics from retailers. The glass fiber fabrics were really thin, 40 µm, it looks like satin but any manipulation without care should displace the fibers and put at stake the manufacturing accuracy. Since process repeatability is considered not good enough, it is impossible to know precisely the mixing ratio, so calculations were run with the mechanical properties of Table 4.1.

Table 4.1: Glass fiber, from HexForce®.

Properties	Value
Nominal weight	48 g/m²
Warp / Weft	56 / 44 %
Weave style	Plain
Finish	TF970
Thickness	0.04 mm

Chosen mechanical properties	Value
Young modulus E_1	26.6 GPa
Young modulus E_2	2.97 GPa
Shear modulus G_{12}	1.39 GPa
Major Poisson ratio	0.4
Minor Poisson ratio	0.045

4.1.2 Resin

A vinylester resin was used, which is a resin produced by the esterification of an epoxy resin with an unsaturated monocarboxylic acid. First, it can cure at room temperature and this is a midway alternative to polyester and epoxy. Then, mechanical properties of vinylester are quite good for a matrix, especially against stretching failure. This makes vinylester more able to absorb impact without damage [19]. The cross bonding of vinylesters is superior to that of polyesters. This means that vinylesters bond to core materials much more effectively than polyesters and delamination is less of an issue.

Table 4.2: Vinylester, from Reichhold®.

Name of the solution	Mass proportion
Dion 9102	100
Accelerator 9802	2
Accelerator 9826	0.5
Inhibitor 9853	0.2
Norpol peroxide 11	2
Gel time, in minutes	43

Mechanical properties	Value
Tensile strength	79 MPa
Tensile modulus	3400 MPa
Tensile elongation	4.5 %
Flexural strength	130 MPa
Flexural modulus	3250 MPa
Heat distortion temperature	100 °C

Nevertheless, this resin cannot go into space because it is sensitive to UV. Moreover, its low glass transition temperature around 100°C cannot resist the sun exposure in space. This is why an epoxy resin, similar to RTM6-2 with high glass transition temperature of 183°C, may resist the solar heat and thermal fatigue, due to the expansion during the day/night phases.

4.1.3 [+45F/−45F/0F/+45F/−45F] layup

Since the fabrics are not balanced (warp direction is 1-direction), for an antisymmetric layout it is necessary to use two woven layers on each side of a woven layer "0/90" in the middle, for a total thickness of 0.20 mm. The corresponding ABD matrix is weak, particularly the bending stiffness matrix which is very low.

Manufactured samples of this layup has revealed that 5 layers were not enough, as the tape spring was too weak in torsion.

$$\begin{bmatrix} \boldsymbol{A} & \boldsymbol{B} \\ \boldsymbol{B} & \boldsymbol{D} \end{bmatrix} = \begin{bmatrix} 2.18 & 1.13 & 0 & 0 & 0 & -0.00344 \\ 1.13 & 2.07 & 0 & 0 & 0 & -0.00344 \\ 0 & 0 & 1.16 & -0.00344 & -0.00344 & 0 \\ 0 & 0 & -0.00344 & 6.39 \cdot 10^{-3} & 4.47 \cdot 10^{-3} & 0 \\ 0 & 0 & -0.00344 & 4.47 \cdot 10^{-3} & 6.38 \cdot 10^{-3} & 0 \\ -0.00344 & -0.00344 & 0 & 0 & 0 & 4.59 \cdot 10^{-3} \end{bmatrix}$$

4.1.4 [+45F/−45F/+45F/−45F/0F/+45F/−45F/+45F/−45F] layup

By adding two new layers to the previous layout, for a total thickness of 0.36 mm, the bending stiffness has been multiplied by six. It is explained with regard to the construction of the $\boldsymbol{D}$ matrix is directly related to the cubic distance from the mid-plane.

$$\begin{bmatrix} \boldsymbol{A} & \boldsymbol{B} \\ \boldsymbol{B} & \boldsymbol{D} \end{bmatrix} = \begin{bmatrix} 3.71 & 2.21 & 0 & 0 & 0 & -0.00688 \\ 2.21 & 3.59 & 0 & 0 & 0 & -0.00688 \\ 0 & 0 & 2.27 & -0.00688 & -0.00688 & 0 \\ 0 & 0 & -0.00688 & 0.0371 & 0.0262 & 0 \\ 0 & 0 & -0.00688 & 0.0262 & 0.0371 & 0 \\ -0.00688 & -0.00688 & 0 & 0 & 0 & 0.0269 \end{bmatrix}$$

Compared to the tape spring features studied in Chapter 2, the transversal radius is 1.65 mm larger but the coiling radius is clearly smaller. According equation (2.7), $R_{\text{coiling}} = 11.3\,\text{mm}$.

4.2 Vacuum molding procedure

4.2.1 Cutting

In preparation for the manufacturing, the table needs to be cleaned and a vacuum bag has to be set onto the table to protect but also to draw lines on it to make easier the rest of the manufacturing steps. After rolling out the fabric, one must make a precise frame with adhesive tape over the fiber. It helps to keep the fiber in place,

then tape again sub-frames which corresponds to the dimensions of the samples. Thus, cutting becomes easier, but using a ruler and a sharp pizza slicer, one should cut in the middle of the tape width to keep the frame all around the piece. In Fig. 4.2, the 45° layers are being cut (pay attention to the reflection on the fabrics).

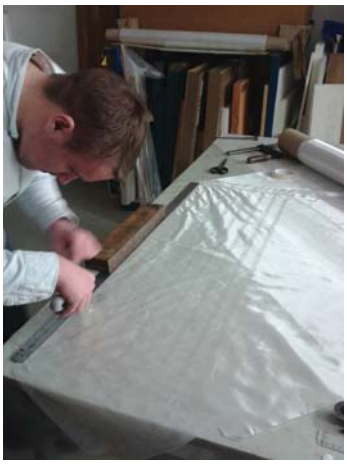

Figure 4.2: Cutting the fabric.

4.2.2 Assembling the layers

As all the 45° layers are cut at the same time, using a legend is mandatory to ensure the layup. One can manipulate the pieces by the frame and then tape all of them onto the peel-ply one on top of the other to form the final layup of the boom, without the resin.

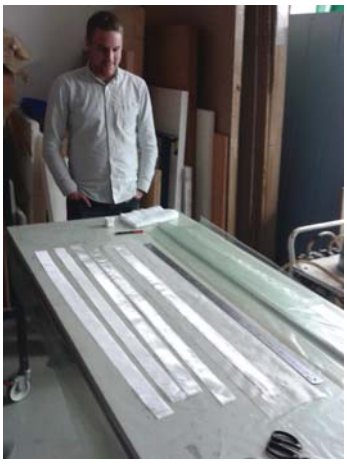

Figure 4.3: Sorting and assembling.

4.2.3 Adding the resin

When the mixing of the vinylester is done, be careful to wait until the end of the chemical reaction in the bucket, otherwise some bubbles might be retained inside the matrix. Since this step, one have to wear a mask for safety reason.

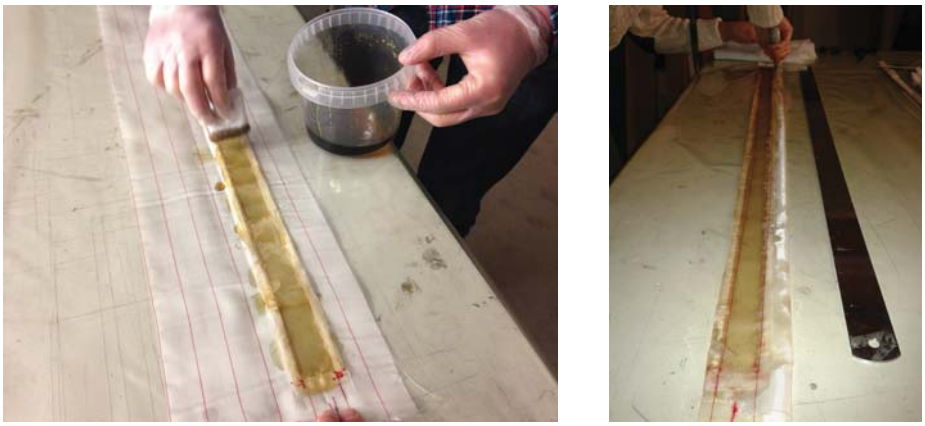

Figure 4.4: Adding the resin and cutting the peel-ply.

A sponge tool is very useful to apply the resin through 5 or 9 layers. Apply the resin from above only, not to displace the layup which has become more flexible with the resin addition. The sponge tool provides the adequate amount of resin by sucking up the excess. Finally the peel-ply, containing the composite laminate, is cut to cover two third of the tube circumference.

4.2.4 Molding

The peel ply is then adjusted onto the copper tube which has been attached on both sides to the table. Release films are added to ensure an easier removal, according to Fig. 4.6. The laminate has to be carefully rolled around the tube, to pre-shape it. One may add the final 120 g/m^2 breather layer over everything and use tacky-tape to close the vacuum bag, in order to avoid leaks. Moreover, to avoid kinks of the vacuum bag, one can decrease slowly the pressure inside the bag and then pull out the bubbles, kinks and wrinkles. This will ensure a better surface finish. Looking for leaks is also important if you want the geometry to be kept when the laminate cures.

With vinylester, the pressure should not go under 0.2 bar otherwise it starts to boil, so the pressure was maintained at 0.4 bar during two hours for curing at room temperature.

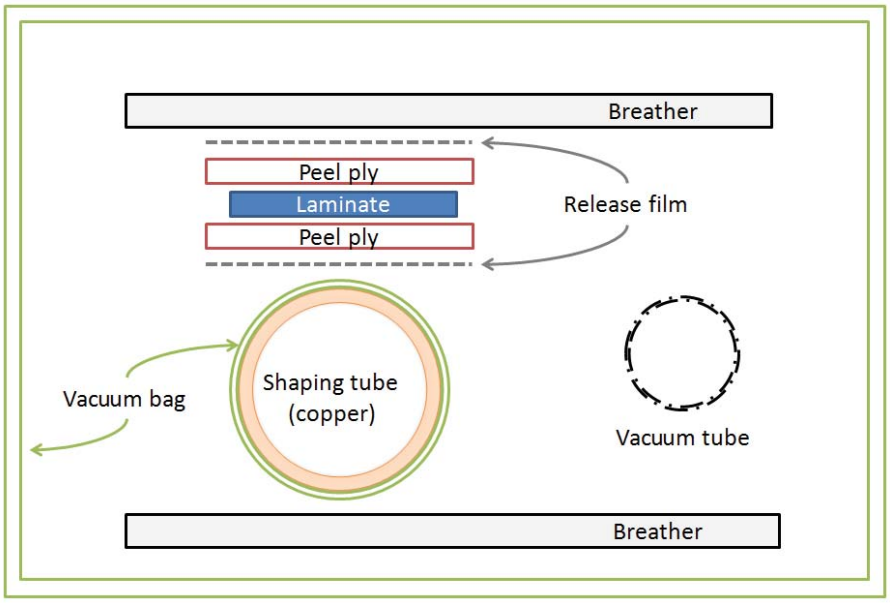

Figure 4.5: Vacuum molding scheme.

Figure 4.6: Vacuum bag containing the laminate and vacuum pump.

4.2.5 Post curing

After two hours or more, a partial curing of the boom is done but post curing at a temperature beyond the glass transition temperature is necessary to ensure a total chemical reaction and a perfect cross-linking, providing better bonds to core materials.

The bag, maintained under pressure, and the tube were placed inside the oven for two more hours at 70°C, with a safety temperature of 90°C in case of the exothermic reaction creates too much heat.

Figure 4.7: Post-curing in an oven.

4.3 Observations and improvements

All manufactured samples were able to coil, one of them was slightly helical and this is due to a misalignment of the fabric on the tube.

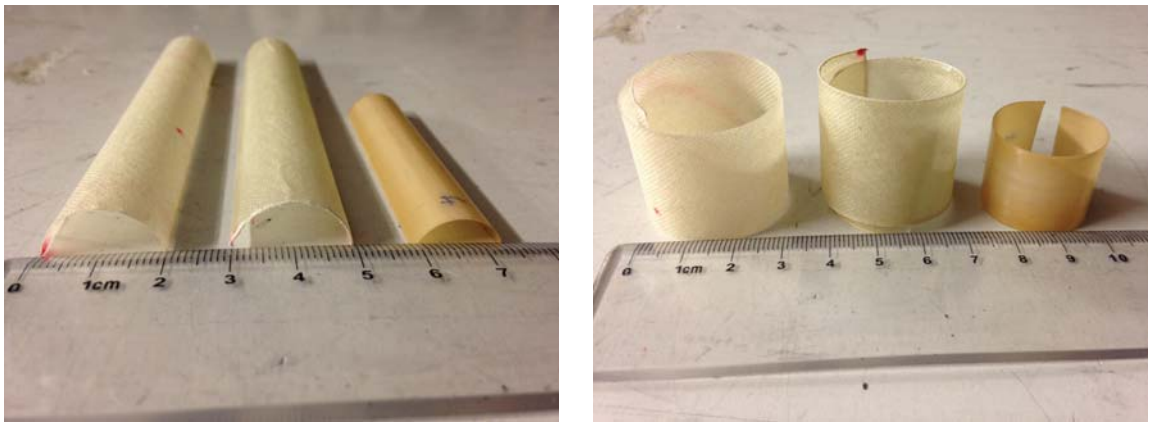

Figure 4.8: Made samples and AFRL tape spring.

Obviously this manual manufacturing process takes a long time. After some training, manufacturing a 1 meter tape spring took 8 hours, i.e. 4 hours to prepare, cut the fabrics and make the laminate, then 4 hours for "baking". One can add that the fiber orientation accuracy is around $\pm 5°$, because of the numerous handling steps.

Vacuum injection molding might be a better alternative because it shall minimize delamination at the edges, Fig. 4.9. Another improvement could be also laser-cutting of the longitudinal edges. Using two molds instead of only one might improve the surface finish and repeatability.

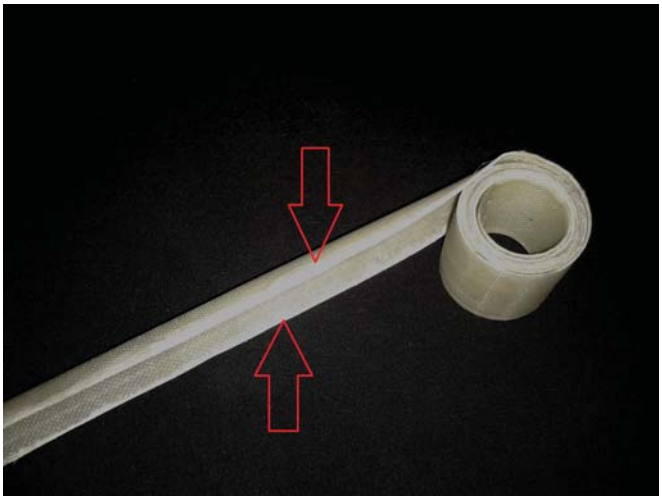

Figure 4.9: Delamination of the tape spring.

5 Next Generation of Glass Fiber tape springs

5.1 Why making a new tape spring?

5.1.1 Deployment issue

Since the made tape springs can coil, why new one should be manufactured? When the tape springs are kept coiled during several hours, then they can no longer deploy by themselves. Not only, when the tape spring is coiled the applied bending causes stiction which prevents the boom from deploying correctly, by itself. But also stress relaxation occurs after some time and a piece of the stored energy is lost in the resin and the fiber realignment.

A project called Bistable Over the Whole Length (BOWL) [9], has shown that a variable fiber orientation could offer different natural coiling radius along the boom. The smaller radii are made with a fiber angle larger than 45°, and conversely.

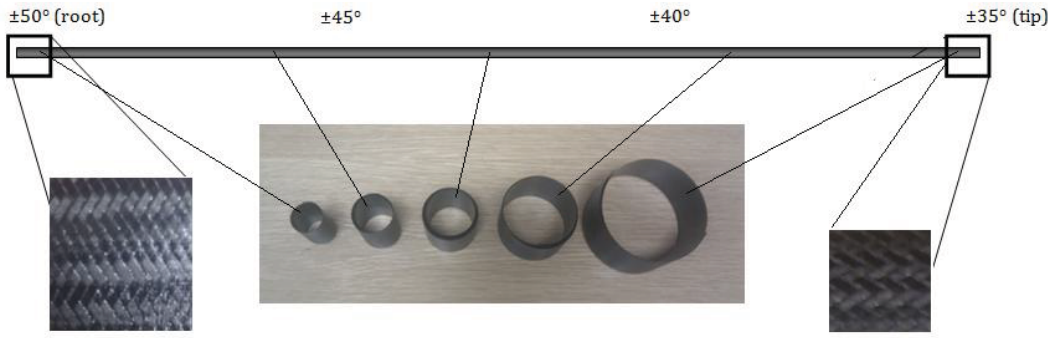

Figure 5.1: BOWL project, $L = 5$m, $R = 25$ mm.

The aim is to adapt the requirements of the 1-meter glass fiber tape spring, all along or just by segments, and also be able to understand the relationship between the growing coiling radius and the variable fiber orientation.

5.1.2 Relation between coiling radius and fiber orientation

In the case of the fiber orientation changes, it would mean the layout is actually [+αF/−αF/+αF/−αF/0F/+αF/−αF/+αF/−αF]. Keep in mind that α represents only the warp, the weft is not mentioned but included. One can sweep α from 0 to 90 and bi-stability is found for an interval from 29° to 61° which corresponds to an interval from 7.3 mm to 27.1 mm for the coiling radius. In Fig. 5.2 and 5.3, one can see the energy plots for α = 32° and 58°.

When α is small, the coiling radius is large and the stored energy is low. A 0° layer has mostly stretching energy when a 90° layer has bending energy. Moreover the stretching contribution is low in term of stored energy, less than 1% at the second stable point. When α increases, the coiling radius decreases but the stored energy increases.

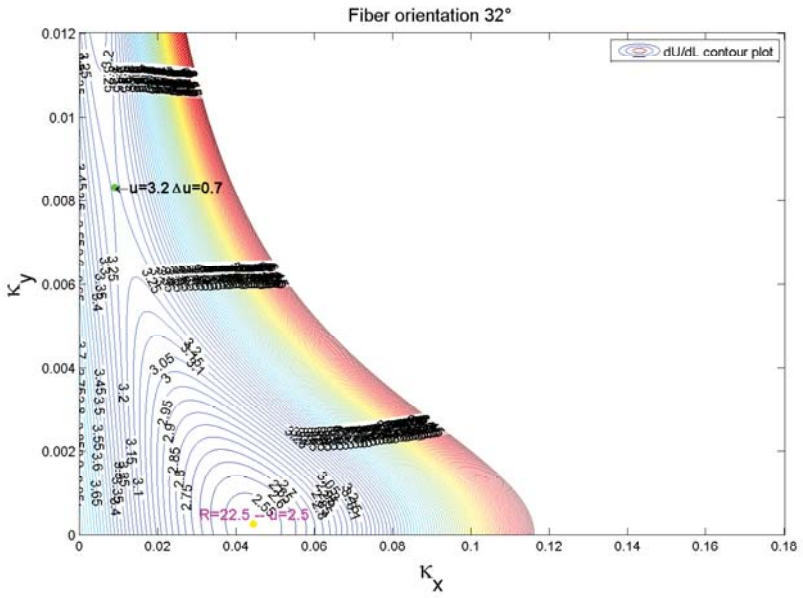

Figure 5.2: Strain energy plots for [+αF/−αF/+αF/−αF/0F/+αF/−αF/+αF/−αF], α = 32° and R = 8 mm.

In Fig. 5.4 the fiber orientation is versus the coiling radius is shown, the curved line fits with an exponential model which parameters depends of the layout and geometric parameters. In the SEAM project, it was decided to have an initial radius of 10 mm. This requirement leads the whole development of the BOWL boom. Using the Archimedes spiral approximation with the equation $R_{\text{coiling}} = \sqrt{tL/\pi + {R_0}^2}$, where t is the thickness and L the boom length, the final coiling radius is 18.14 mm, so 11.3 loops or coils. In the zoomed plot, every x-axis graduation corresponds to one coil so the optimal fiber orientation can be read for each coil.

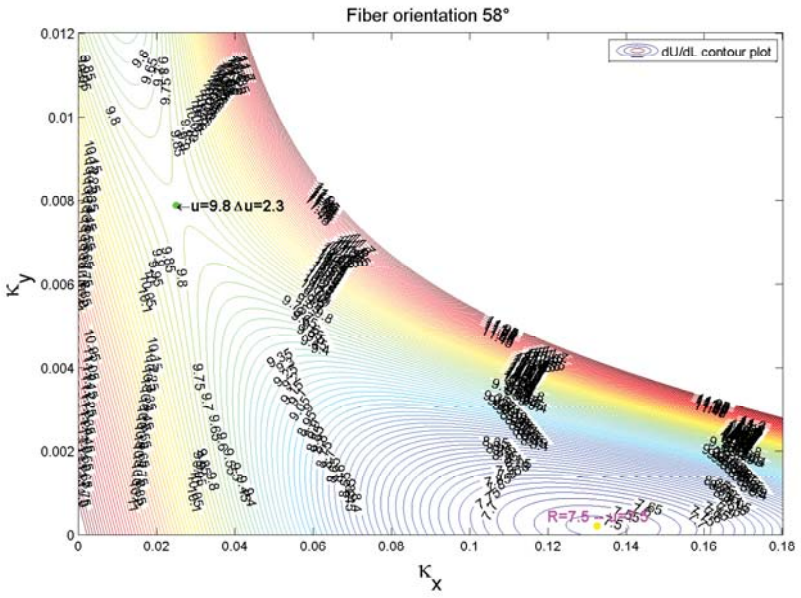

Figure 5.3: Strain energy plots for [+αF/−αF/+αF/−αF/0F/+αF/−αF/+αF/−αF],α = 58° and $R = 8$ mm.

5.2 What will it change?

5.2.1 Deployment force and time

Since the layup changes all along the boom, the released energy also changes. Jeon and Murphey [10] founded a simple relation between the ideal deployment separation force and the stored strain energy at a stable point (without friction). For the case of a BOWL's type boom, this is equivalent to equation (5.1) where r is the coiling radius:

$$F(r) = \frac{dU}{dL}(r) \tag{5.1}$$

It is really convenient to plot the deployment force with respect to the coiling radius (or fiber orientation). In the terms of stored energy, the deployment force increases with the fiber orientation. It means the boom accelerates more at the end than at the beginning of the deployment. As one can see in Fig. 5.5, the minimum force is 2.69 N and the final force is 4.21 N. To compare, during a classic boom [45/0/45] deployment, acceleration decreases with time.

The ideal deployment time can be calculated thanks to Q, the bending strain energy to pass from straight to coiled configuration, equation (5.2). Tibert and Mallol [20]

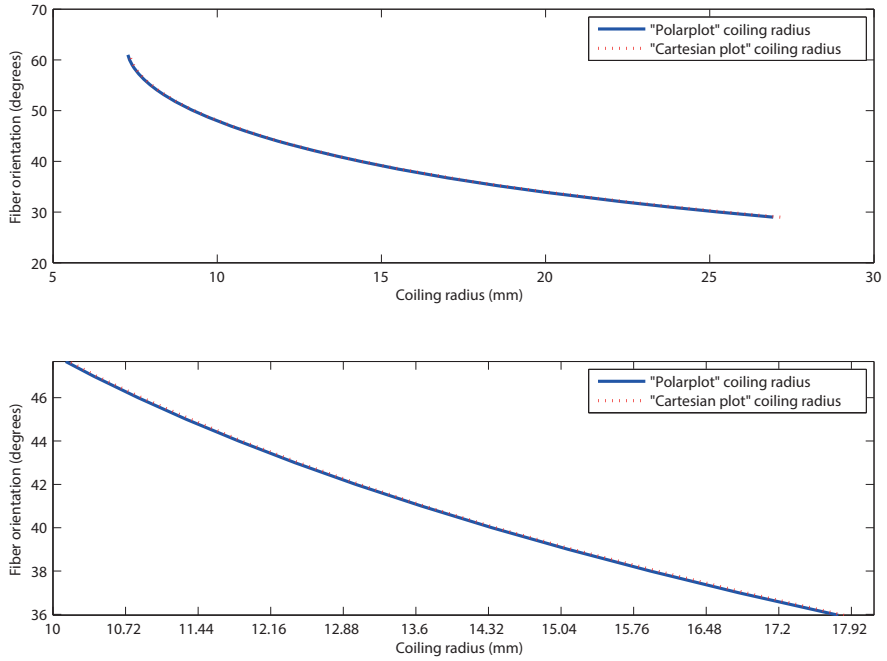

Figure 5.4: Fiber orientation according to the coiling radius.

have developed a model which also include φ_{cf}, the final angular rotation of the tape spring, equation (5.3).

$$Q(r) = \frac{F(r)r}{4L} \tag{5.2}$$

$$\phi_{cf} = \frac{\pi}{t}(r_{final} - r_0 - \frac{t}{2}) \tag{5.3}$$

It takes into account two tape springs pushing the sensor, weighting 0.048 kg, away from the satellite main structure. The calculations of equation (5.4) have shown that the deployment takes 0.31 s. To compare again, a boom with layup [±45/0/±45] can deploy in 0.27 s.

$$\Delta t = \frac{1}{L}\int_0^L \frac{r^2\phi_{cf}2m_{sensor}}{Q(r)}dL = \int_0^L \frac{8r\phi_{cf}m_{sensor}}{F(r)}dL \tag{5.4}$$

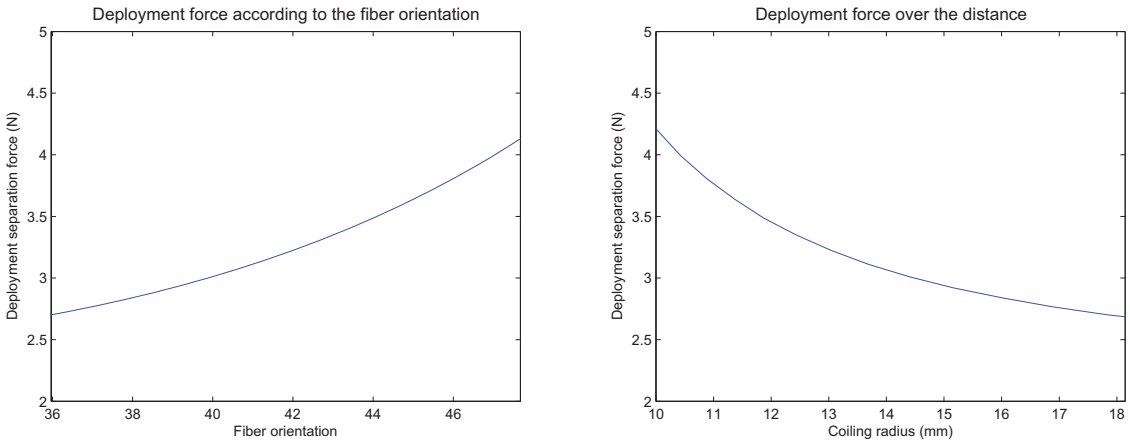

Figure 5.5: Deployment forces according to the fiber orientation and to the coiling radius of [+αF/−αF/+αF/−αF/0F/+αF/−αF/+αF/−αF] layout, $R = 8$ mm.

To make a brief conclusion, the new tape springs deploy slightly slower than those with no fiber orientation change and also have a larger bending stiffness. Nevertheless, the force increases during the deployment which may increase the shock-wave and displacement generated.

5.2.2 Equivalent isotropic Young's modulus

Since the fiber changes along the boom, the mechanical properties as well. For instance, the longitudinal Young's modulus is around 14 GPa at the sensor edge but only 9 GPa at the clamped edge.

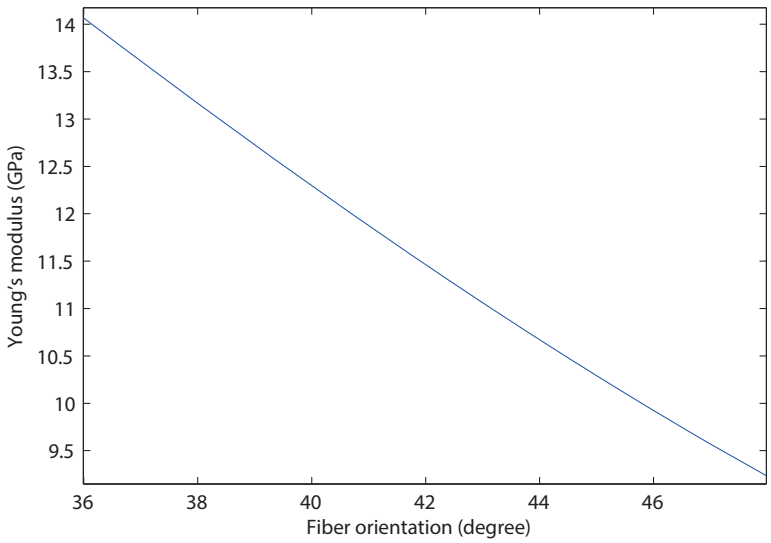

Figure 5.6: Young's modulus along the boom for [+αF/−αF/+αF/−αF/0F/+αF/−αF/+αF/−αF] layout, R= 8 mm.

6 Conclusion

Deployable structures are essential for satellite and there is trend towards minimizing them and tape spring boom is a lightweight solution. Bi-stability comes from the use of composite materials and the Matlab code can model the mechanical properties, the stored energy, with a simple woven model where plenty of parameters are envolved.

The preliminary tests drew confusing conclusions since the natural coiling radius was below the computed one. From another side, the tape spring has a large stability range, it naturally coils at a radius of 12.1 mm and snaps at a radius of 20.0 mm, representing an increase of 66% for the material and layout tested.

Manufacturing of several dry fabric plies is a tedious work and its long process gives a fair quality for man made tape spring, in terms of finish and bi-stability. Nevertheless, accuracy, repeatability and delamination need to be improved by a new process or an industrial background. The main drawback comes from the really thin dry unbalanced fabrics. Yet the 9-layer tape spring is interesting in many aspects. It is stiff, both in bending and torsion, but the tape spring is too much stable and has trouble in deploying, because it is neutrally stable.

The advanced model with a changing Young's modulus, adapted from BOWL, explain at once advantages and drawbacks of changing fiber orientation. Even with a smaller deployment time, the inceasing acceleration of the booms could jeopardize the sensors. But at least, thanks to the sweeping of the fiber orientation, you can choose the initial coiling radius when the bulk is a requirement.

Acknowledgments

I would like to thank my supervisor Dr. Gunnar Tibert for giving me the opportunity to work on this exciting project and his precious help.

I want to thank Pau Mallol (PhD student at KTH) for the relevant conversations, his support throughout the whole project.

I do not forget Anders Beckman, with whom it was a pleasure to run experiments and manufacture composites.

I would not have managed to write this thesis report without the KTH's staff and the help of my colleagues, for their own expertise, but also for the enjoyable hours spent.

Bibliography

[1] "Wikipedia, (2014). CubeSat. [online] Available at: http://en.wikipedia.org/wiki/cubesat [Accessed 12 Dec. 2014] ."

[2] "02Gr733, E. (2014). AAU CUBESAT - Student Satelitte. [online] Space.aau.dk. Available at: http://www.space.aau.dk/cubesat/ [Accessed 29 Jan. 2014]."

[3] "Nasa.gov, (2014). NASA - GeneSat-1. [online] Available at: http://www.nasa.gov/centers/ames/missions/2007/genesat1.html [Accessed 29 Jan. 2014]."

[4] I. A. Arriaga Trejo, "Numerical modeling and evaluation of the small magnetometer in low-mass experiment (smile)," Master's thesis, Space and Plasma Physics Royal Institute of Technology, 2007.

[5] "Small Explorer for Advanced Missions, SEAM, project coordinator: Dr. Nickolay Ivchenko, KTH, Stockholm."

[6] M. M. Mikulas, T. J. Collins, W. Doggett, J. Dorsey, and J. Watson, "Truss performance and packaging metrics," in *AIP Conf. Proc., vol. 813, pp. 1000-1009*, 2006.

[7] F. Jensen and S. Pellegrino, "Arm development review of existing technologies," in *CUED/D-STRUCT/TR 198 NSE/GNSR/5031 Contact reference No. 400 43169*, 2001.

[8] D. Zenkert and M. Battley, *Foundations of Fibre Composites*. Paper 96-10 Second edition, revised, 2003.

[9] J. M. Fernandez, A. Viquerat, V. J. Lappas, and A. J. Daton-Lovett, "Bistable over the whole length (BOWL) CFRP booms for solar sails," in *Surrey Space Centre, University of Surrey, Guildford, Surrey, GU2 7XH, UK and RolaTube Technology Ltd., 130 Wellworthy Road, Ampress Park, Lymington, Hampshire, SO41 8JY, UK*, 2013.

[10] S. K. Jeon and T. W. Murphey, "Design and analysis of a meter-class cubesat boom with a motor-less deployment by bi-stable tape springs," in *CSA Engineering, Albuquerque, NM, USA and Air Force Research Laboratory, Space Vehicles Directorate, Kirtland AFB, NM, USA*, 2010.

[11] Y. Prigent, "A finite element model of bi-stable woven composite tape-springs," Master's thesis, Royal Institute of Technology, 2011.

[12] K. Iqbal and S. Pellegrino, "Bi-stable composite shells," in *Department of Engineering, University of Cambridge, Trumpington Street, Cambridge, CB2 1PZ, U.K.*, 2000.

[13] S. Guest and S. Pellegrino, "Analytical models for bistable cylindrical shells," in *Department of Engineering, University of Cambridge, Trumpington Street, Cambridge CB2 1PZ, UK*, 2006.

[14] N. K. Naik and V. K. Ganesh, "An analytical method for plain weave fabric composites," tech. rep., Composites, vol. 26, pp. 281-289., 1995.

[15] M. A. Meyers and K. K. Chawla, *Mechanical Behavior of Materials*. Cambridge University Press; Second edition (December 8, 2008), 2008.

[16] "Wikipedia, (2014). Creep (deformation). [online] Available at: http://en.wikipedia.org/wiki/Creep (deformation) [Accessed 5 Feb. 2014]."

[17] D. Roylance, "Laminated composite plates," tech. rep., Department of Materials, Science and Engineering Massachusetts Institute of Technology, Cambridge, MA 02139, 2000.

[18] "Wikipedia, (2014). Stress relaxation. [online] Available at: http://en.wikipedia.org/wiki/Stress relaxation [Accessed 5 Feb. 2014]."

[19] "Johnson, T. (2014). Vinyl Ester vs Polyester Resins. [online] About.com Composites / Plastics. Available at: http://composite.about.com/od/Resins/a/Vinyl-Ester-Vs-Polyester-Resins.htm [Accessed 15 Dec. 2013]."

[20] P. Mallol Parera and G. Tibert, "Deployment modeling and experimental testing of a bi-stable composite boom for small satellites," in *Proceedings of the 54th AIAA/ASME/ASCE/AHS/ASC Structures, Structural Dynamics, and Materials Conference*, Boston, MA, 8-11 April 2013.